Available online at www.sciencedirect.com
ScienceDirect
Ceramics International 35 (2009) 787–790
CERAMICS INTERNATIONAL
www.elsevier.com/locate/ceramint

Crystal structure of Ce-doped $CaMnO_3$ perovskite

J. Dukić *, S. Bošković, B. Matović

Institute of Nuclear Sciences "Vinča", Materials Science Laboratory, Mihajla Petrovića Alasa 12-14, P.O. Box 522, 11001 Belgrade, Serbia

Received 12 December 2007; received in revised form 27 January 2008; accepted 20 February 2008
Available online 4 July 2008

Abstract

The synthesis and crystal structure of Ce-doped $CaMnO_3$ perovskite has been investigated. Two powders with nominal compositions $Ca_{0.5}Ce_{0.5}MnO_3$ and $CaMn_{0.5}Ce_{0.5}O_3$ were prepared using a modified glycine/nitrate procedure. The possibility of incorporation of Ce ions in the positions A and B of the perovskite structure was investigated by X-ray methods. Influence of Ce on unit cell volume of the perovskite compounds, occupation numbers and distances between atoms were analyzed by Rietveld refinement. Microstructure size–strain analysis was performed, as well. The results revealed that Ce entered both positions A and B in the structure.

Keywords: B. X-ray methods; D. Perovskite

1. Introduction

Doped perovskite manganites, with a general formula of $A_x^{2+}Re_{1-x}^{3+}Mn_x^{4+}Mn_{1-x}^{3+}O_x^{2-}$ (A: alkali earth element, Re: rare earth element), have attracted considerable interest due to their colossal magnetoresistance [1]. In Re-doped manganites, Mn exists both as Mn^{3+} and Mn^{4+} in order to maintain the charge neutrality of the compound. The dopant will either occupy the A site, the B site, or both A and B sites (amphoteric) of the perovskite, depending on the Re radius. Typically, the larger Re atoms will occupy A sites, while the smaller cations prefer the B sites.

The valence of dopants is influenced by the surroundings [2]. A site drives the rare earth towards lower valence, while B site drives it towards higher valence. In cerium-doped manganites, since Ce is a multivalent cation, it is possible for Ce^{3+} and Ce^{4+} species to coexist in the same compound, adding an extra source of structural disorder. The partition is influenced by the A/B ratio that is to some extent affected by oxygen partial pressure.

Today, the experimental data on cerium-doped manganites available in the literature are limited and not conclusive in various aspects. There are few studies about these compounds, but none of the papers have taken the possibility of multiple valence states of Ce into account. In particular, the question about the valence state of Ce ions in these compounds is still an open matter [3,4].

The Ce^{4+} as a dopant cation for $CaMnO_3$ was chosen as its size is fairly close to that of Ca^{2+}. Each Ce^{4+} substituted for Ca^{2+} can potentially donate two electrons into the conduction band of insulating $CaMnO_3$ [3]. For air-prepared samples, the most stable valence state of cerium is expected to be 4+ [5]. Therefore, charge neutralization would require the formation of Mn^{2+}. On one hand, Mn^{2+} is much larger cation than Mn^{3+} and Mn^{4+}; on the other hand, Ce^{4+} is a much smaller ion then the Ce^{3+}. Both effects led to very low Goldschmidts tolerance factor [6] whose value is 0.907 for cerium ions in the 4+ charge state. This fact indicates that the cerium-doped structure is very unstable and, as a consequence, CeO_2 segregation could have occurred.

However, a detailed crystal structure analysis shows that even the samples prepared through the precipitation method show a secondary phase which predominantly corresponds to CeO_2. For example, according to Ref. [5] if less than 0.6 wt.% of cerium oxide is segregated, only 3.6% of cerium ions are out of the perovskite compound. Although the reasons for CeO_2 segregation in these samples are not well established, it may be related to the presence of Ce^{4+} cations.

* Corresponding author. Present address: Technische Universität München, Tectonics and Material Fabrics Section, Arcisstraße 21, 80333 München, Germany. Tel.: +49 89 28925885; fax: +49 89 28925852.
E-mail addresses: jelena@vin.bg.ac.yu, jelena.dukic@mytum.de (J. Dukić), boskovic@vin.bg.ac.yu (S. Bošković), mato@vin.bg.ac.yu (B. Matović).

0272-8842/$34.00
doi:10.1016/j.ceramint.2008.02.023

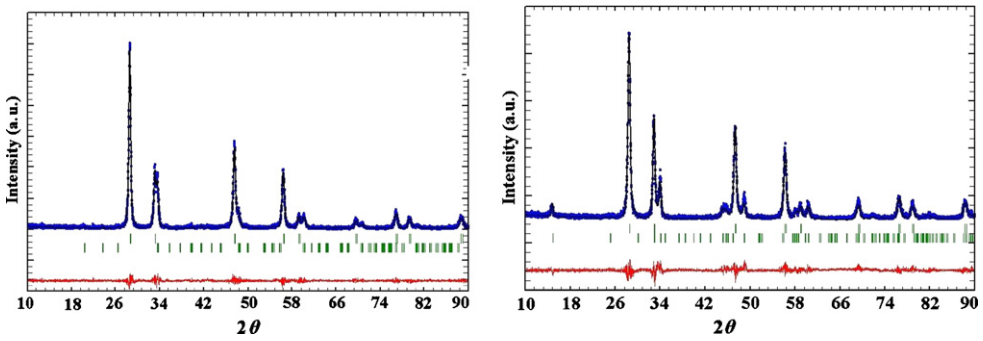

Fig. 1. Results of Rietveld refinement of the samples: (a) Ca50 and (b) Mn50.

Main goal of this work is to investigate the possibility to form nanostructured solid solutions with nominal compositions $Ca_{0.5}Ce_{0.5}MnO_3$ and $CaMn_{0.5}Ce_{0.5}O_3$ using a modified glycine/nitrate procedure (MGNP) and to analyze more precisely their crystal structures.

2. Experimental

Powders of nominal composition $Ca_{0.5}Ce_{0.5}MnO_3$ (Ca50) and $CaMn_{0.5}Ce_{0.5}O_3$ (Mn50) were prepared using a modified glycine/nitrate process. Aminoacetic acid (glycine) was used as a fuel, while the metal-nitrate was an oxidant [7]. After synthesis samples were calcined at 800 °C for 3 h.

The phases of samples were identified using X-ray powder diffraction (XRPD) on a SiemensD500 diffractometer with a Ni filter using Cu Kα radiation and the step-scan mode (2θ-range: 10–90°). To derive the relevant structural parameters, the experimental data for Rietveld refinement were taken afterwards over an angular range 10–90° 2θ, with a step width of 0.02° and 10 s/step. Structural analysis was carried out using Rietveld refinement and the program FullProf [8].

3. Results and discussion

XRPD analysis of the calcined powders revealed two-phase compositions for the investigated samples. Ca50 sample consists of two crystalline phases (perovskite and CeO_2), as well as Mn50 sample (Ca_2MnO_4 and CeO_2). The best fits between calculated and observed X–ray diffraction patterns for Ca50 and Mn50 samples are given in Fig. 1. All allowed Bragg reflections are shown by vertical bars. By inspecting difference between the experimental and calculated profiles, good agreement can be observed.

In the Ca50 sample, crystalline phases are CeO_2 and Ce-doped $CaMnO_3$. Quantitative phase analysis revealed that CeO_2 is the more abundant phase with 58.7(4) mass%. The results of Rietveld analysis, i.e., unit cell parameters, unit cell volume and microstructure parameters are summarized in Table 1. Refined unit cell parameter of CeO_2 is 5.3990(5) Å, which is smaller than for pure ceria, i.e. 5.4112(10) Å [9]. Ceria nanopowders often show increase of unit cell parameter as the result of introducing Ce^{3+} (1.143 Å) instead of Ce^{4+} (0.97 Å) in the structure, but that is not the case here. Average Ce–O distance, ⟨2.338 Å⟩ is shorter than literature value of 2.343 Å [9] also indicating the presence of smaller cation in the structure. The only cations that are present in Ca50 sample and whose ionic radii for coordination number (CN) = 8 is smaller than Ce^{4+} are the Mn ions. Thus, any incorporation of Mn ions on the Ce^{4+} site could result in decreasing of lattice parameter due to smaller ionic radius of Mn (Mn^{2+} = 0.83 Å, Mn^{3+} = 0.645 Å and Mn^{4+} = 0.53 Å) which is smaller than that of Ce^{4+} (0.97 Å). Introducing Mn in the structure and performing Mn, Ce occupation factor refinement, gave us an improved structural model, on the basis of which we found that 2.7% of Mn was in 4a position of the fluorite structure-type ceria.

The second phase in Ca50 sample is the perovskite phase, doped $CaMnO_3$, and results of refinement for this phase are given in Table 1. Table 2 contains refined atomic parameters.

Table 1
Results of Rietveld refinement

	Sample			
	Ca50		Mn50	
	CeO_2[a]	$Ca_{1-x}Ce_xMnO_3$[a]	CeO_2[a]	Ca_2MnO_4[a]
Unit cell parameters (Å) and volume (Å^3)	a = 5.3990(5), V = 7.380(7)	a = 5.324(5), b = 7.508(4), c = 5.341(5), V = 213.5(3)	a = 5.4201(2), V = 159.23(1)	a = 5.2567(6), b = 5.2567(6), c = 23.809(5), V = 657.9(2)
Microcrystalline size (Å)	222.3(1)[b]	169.4(3)[b]	173.65(8)[b]	153.4(2)[b]
Microstrain	0.022691(2)[b]	0.04247(4)[b]	0.02030(1)[b]	0.02578(4)[b]

[a] Phases.
[b] Values in brackets are a measure of the degree of anisotropy.

Table 2
Refined atomic parameters results

	Sample	
	Ca50, $Ca_{1-x}Ce_xMnO_3$[a]	Mn50, Ca_2MnO_4[a]
Ca site		
x	0.016(3)	0
y	0.25	0.25
z	−0.000(3)	0.5516(2)
Occ (%)		
Ca	84.2	48.4
Ce	15.8	52.4
Mn site		
x	0	0
y	0	0.25
z	0.5	0.375
Occ (%)		
Mn	95	
Ce	5	
O1 site		
x	0.424(9)	0
y	0.25	0.25
z	0.172(9)	0.469(2)
O2 site		
x	0.25(1)	0.588(4)
y	0.027(2)	0.838(4)
z	−0.26(1)	0.125

[a] Phases.

Ce-doped $CaMnO_3$ crystallizes in the space group *Pnma* and its structure obtained as a result of refinement is given in the Fig. 2a. Unit cell volume of this phase is 213.5(3) $Å^3$, and it is increased as compared to undoped $CaMnO_3$ [10]. This indicates Ce^{3+} presence in the structure. Ionic radius of Ce^{3+} (1.14 Å) is close to Ca^{2+} (1.12 Å). As a result of entering Ce^{3+} in the structure, a small increase of unit cell volume can be expected. Doping with Ce^{3+} results in a reduction of an equivalent amount of Mn^{4+} (0.53 Å) to Mn^{3+} (0.645 Å) with larger ionic radius, and this is another mechanism that contributes to the unit cell volume increase. Independently of the relatively large difference in ionic radii between Mn and Ce ions in VI coordination, literature data claim that Ce gets incorporated into the position B [11]. Occupation factors refinement gave us 15.8% of Ce in the position A and 5% in the position B of the perovskite structure. Since the applied method cannot give informations about Ce valence state we could expect Ce^{3+} ions in the Ca site and Ce^{4+} ions in the Mn site, based on ionic radii of these cations.

The ⟨Mn–O⟩ bond length in undoped $CaMnO_3$ [9] is 1.899 Å, after refinement 1.977 Å is obtained as an average Mn–O distance, indicating also the presence of Mn^{3+} and Ce in the structure, since average distance Ce^{4+}–O in octahedral coordination is 2.239 Å [12].

XRPD of sample Mn50 shows the present of CeO_2 as a dominant phase, as well as Ca_2MnO_4 phase. Obtained ceria phase has larger unit cell (5.4201(2) Å) as compared to pure ceria. This increase of unit cell parameters of the CeO_2 may be a consequence of reduction in the valent state of Ce^{4+} ions into Ce^{3+} ions followed by increased concentration of oxygen vacancies, that is usually the case with ceria nanopowders [13]. Since ionic radius of Ce^{3+} (1.14 Å) is close to Ca^{2+} (1.12 Å), it is difficult to find contribution of each ion in increasing of the unit cell volume. It is confirmed by introducing Ca in the structure since it did not result in improved structural model.

The other phase Ca_2MnO_4 has a tetragonal K_2NiF_4-type of the structure with the $I4_1/acd$ space group [14,15]. MnO_6 octahedra share corners to form layers that are interleaved CaO layers in the *c*-direction (Fig. 2b). If we compare this and the perovskite structure type we can see that perovskite forms a three-dimensional octahedra net, while Ca_2MnO_4 consists of a two-dimensional perovskite-type array. Results of Rietveld refinement are included in Tables 1 and 2. Calculated unit cell volume of Ca_2MnO_4 is higher then in reference [16] where it is 647.87 Å. The data from Ref. [15] were used as the starting model for refinement that indicated the presence of dopants in the structure. Occupation factor refinement shows that Ca shares the position with Ce (52.4%). This dopant causes the

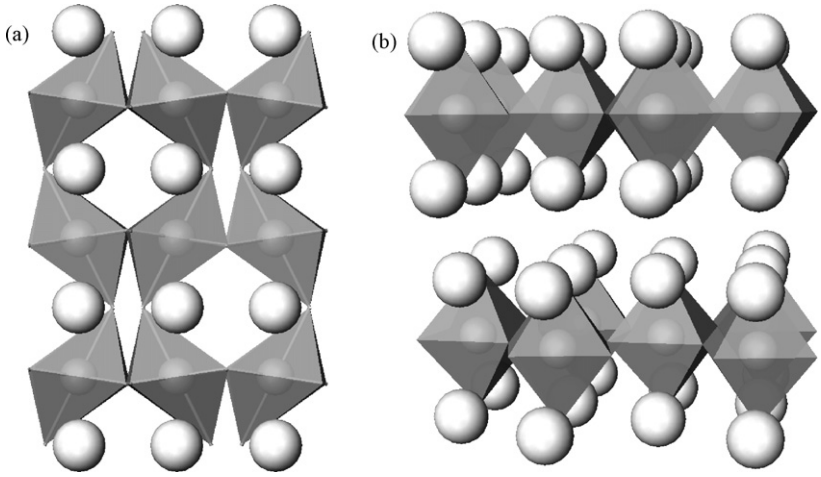

Fig. 2. (a) Crystal structure of $Ca_{1-x}Ce_xMnO_3$ and (b) crystal structure of Ca_2MnO_3. White spheres denote Ca in the Mn–O octahedral net.

reduction of Mn^{4+} into Mn^{3+} and the increase of unit cell volume. Calculated value for ⟨Mn–O⟩ distance is 1.956 Å, and reason for this increase is the presence of Ce^{3+} and Mn^{3+} in the structure.

Line-broadening analysis was performed using the Rietveld method in conjunction with Warren–Averbach procedure in order to get crystallite size and lattice micro-strain parameters. In the present approach, the grain size broadening was represented by a Lorentzian function, and micro-strain broadening by a Gaussian function. The convolution of these functions is a pseudo-Voigt function which is approximated by a modified Thompson–Cox–Hastings pseudo-Voigt [17]. Obtained crystallite sizes are in the nanometric range with crystallites between 150 and 230 Å (Table 1).

The presence of CeO_2, as the major phase indicates that the synthesis conditions used are not adequate for preparation of these particular compositions.

4. Conclusions

Using a modified glycine/nitrate procedure, nanopowders of the nominal compositions $Ca_{0.5}Ce_{0.5}MnO_3$ (Ca50) and $CaMn_{0.5}Ce_{0.5}O_3$ (Mn50) were synthesized. In both samples, two crystalline phases were detected. XRPD pattern of Ca50 sample showed the presence of orthorhombic Ce-doped $CaMnO_3$ perovskite and free ceria, and free ceria and Ca_2MnO_4 in Mn50 sample.

As a result of doping $CaMnO_3$ with Ce, two phases appeared, as well as the occurrence of reduction of Mn^{4+} to larger Mn^{3+} in the B site of perovskite phase. Rietveld refinement showed that Ce enters position A instead of Ca and position B where it changes to some extent the Mn cation in the structure. Unit cell volume and average Mn–O bond distances analyses confirmed the results of Rietveld refinement. Under these experimental conditions we could not synthesize $CaMn_{0.5}Ce_{0.5}O_3$ nominal composition, as well. Instead of single-phase perovskite structure, the Ca_2MnO_4 phase with Ce changing some amount of Ca, as well as free ceria were obtained.

Amount of cerium added to form solid solutions, overcomes solubility limits in both cases, under the experimental conditions applied in this study.

The obtained Ca50 and Mn50 powders are in nanometric range, what is confirmed by the microstructural analysis.

Acknowledgement

This paper has been financially supported by the Ministry of Science and Environmental Protection of the Republic of Serbia, as a part of project No. 142003.

References

[1] C. Krishnamoorthy, K. Sethupathi, V. Sankaranarayanan, R. Nirmala, S.K. Malik, Magnetic and magnetotransport properties of Ce doped nanocrystalline $LaMnO_3$, J. Alloy. Compd. 438 (2007) 1–7.
[2] Y. Tsur, T.D. Dunbar, C.A. Randall, Crystal and defect chemistry of rare earth cations in $BaTiO_3$, J. Electroceram. 7 (2001) 25–34.
[3] Z. Zeng, M. Greenblatt, M. Croft, Charge ordering and magnetoresistance of $Ce_{1-x}Ce_xMnO_3$, Phys. Rev. B 63 (2001) 224410.
[4] J.S. Kang, Y.J. Kim, B.W. Lee, C.G. Olson, B.I. Min, The valence state of Ce in electron-doped manganites: $La_{0.7}Ce_{0.3}MnO_3$, J. Phys.: Condens. Matter 13 (2001) 3779–3789.
[5] G. Alejandro, D.G. Lamas, L.B. Steren, J.E. Gayone, G. Zampieri, A. Caneiro, M.T. Causa, M. Tovar, Strongly frustrated magnetism and colossal magnetoresistance in polysrystalline $La_{0.47}Ce_{0.20}Ca_{0.33}MnO_3$, Phys. Rev. B 67 (2003), 064424.
[6] M. Mogensen, D. Lybye, N. Bonanos, P.V. Hendriksen, F.W. Poulsen, Factors controlling the oxide ion conductivity of fluorite and perovskite structured oxides, Solid State Ionics 174 (2004) 279–286.
[7] S.B. Bošković, B.Z. Matović, M.D. Vlajić, V.D. Krstić, Modified glycine nitrate procedure (MGNP) for the synthesis of SOFC nanopowders, Ceram. Int. 33 (2007) 89–93.
[8] J. Rodriguez-Carvajal, Collected Abstract Of Powder Diffraction Meeting, Toulouse, 1990, pp. 127.
[9] E.A. Kuemmerle, G. Heger, J. Solid State Chem. 147 (1999) 485–500.
[10] H. Taguchi, M. Sonoda, M. Nagao, Relationship between angles Mn–O–Mn and electrical properties of orthorombic perovskite-type $(Ca_{1-x}Sr_x)MnO_3$, J. Solid State Chem. 137 (1998) 82–86.
[11] T.D. Dunbar, W.C. Warren, B.A. Tuttle, C.A. Randall, Y. Tsur, Electron paramagnetic resonance investigations of lanthanide-doped batium titanate: dopant site occupancy, J. Phys. Chem. B 108 (2004) 908–917.
[12] F. Genet, S. Loridant, C. Ritter, G. Lucazeau, Phase transitions in $BaCeO_3$: neutron diffraction and Raman studies, J. Phys. Chem. Solids 60 (1999) 2009–2021.
[13] M. Nolan, J.E. Fearon, G.W. Watson, Oxygen vacancy formation and migration in ceria, Solid State Ionics 177 (2006) 3069–3074.
[14] C. Autret, C. Martin, M. Hervieu, R. Retoux, B. Raveau, G. André, F. Bourée, Structural investigations of Ca_2MnO_4 by neutron powder diffraction and electron microscopy, J. Solid State Chem. 177 (2004) 2044–2052.
[15] H. Taguchi, Electrical property of K_2NiF_4 type $Ca_2(Mn_{1-x}Nb_x)O_4$, Mater. Res. Bull. 36 (2001) 1361–1367.
[16] M.E. Leonowicz, K.R. Poeppelmeier, J.M. Longo, Structure determination of Ca_2MnO_4 and $Ca_2MnO_{3.5}$ by X-ray and neutron methods, J. Solid State Chem. 59 (1985) 71–80.
[17] R.A. Young, The Rietveld Method, IUCr Monographs on Crystallography, Oxford, UK, vol. 5, 1996, pp. 132–166.